Recursive methods for computing the Abel transform and its inverse

Eric W. Hansen and Phaih-Lan Law*

Thayer School of Engineering, Dartmouth College, Hanover, New Hampshire 03755

Received June 25, 1984; accepted November 26, 1984

The Abel transform and its inverse appear in a wide variety of problems in which it is necessary to reconstruct axisymetric functions from line-integral projections. We present a new family of algorithms, principally for Abel inversion, that are recursive and hence computationally efficient. The methods are based on a linear, space-variant, state-variable model of the Abel transform. The model is the basis for deterministic algorithms, applicable when data are noise free, and least-squares-estimation (Kalman filter) algorithms, which accommodate the noisy data case. Both one-pass (filtering) and two-pass (smoothing) estimators are considered. In computer simulations, the new algorithms compare favorably with previous methods for Abel inversion.

1. INTRODUCTION

The problem of reconstructing a two-dimensional function from line integrals, or projections, occurs in a remarkable variety of disciplines in engineering and science. The most well-known application is medical computed tomography, but similar techniques are used for problems ranging from microscopy to astrophysics. A special case of the reconstruction problem is the Abel transform, which results when the function being projected is axisymmetric (dependent on radius alone). With reference to Fig. 1, the axisymmetric function of interest, denoted $f(r)$, is integrated along straight line paths to produce the projection $g(R)$; because of the symmetry, all projections are identical, and one such measurement suffices for reconstruction. The projection is related to the original function by the forward Abel transform[1]

$$g(R) = 2\int_R^\infty \frac{f(r)r\mathrm{d}r}{(r^2 - R^2)^{1/2}}. \tag{1}$$

The reconstruction of $f(r)$ from $g(R)$ is given by the inverse Abel transform; two common forms are[1,2]

$$f(r) = -\frac{1}{\pi}\int_r^\infty \frac{g'(R)\mathrm{d}R}{(R^2 - r^2)^{1/2}} \tag{2a}$$

and

$$f(r) = -\frac{1}{\pi}\frac{\partial}{\partial r}\int_r^\infty \frac{rg(R)\mathrm{d}R}{R(R^2 - r^2)^{1/2}}. \tag{2b}$$

In this paper we treat the problem of computing the Abel inversion, Eqs. (2), for both noiseless and noisy data. The methods proposed are *recursive* in form: Each succeeding point of the Abel inversion is computed from the previously computed point and a new data point. In the noiseless case, the reconstruction filter is a recursive implementation of Eq. (2a). For noisy data, a least-squares approach is taken, and the reconstruction is accomplished by a Kalman filter. The algorithms are efficient [$O(KN)$ for noiseless data and at most $O(K^2N)$ for data with noise, where $K = 9$ and N is the number of data points] and accurate.

The paper is organized as follows. In Section 2, we review applications of the Abel transform and previous approaches to the problem. In Section 3, we develop the theoretical foundation of the method, i.e., the recursive, state-variable models of the Abel transform and its inverse. In Section 4, we present results of a deterministic inverse filter operating on ideal (noiseless) data. We also comment on its performance in the presence of noise and note that it suffers the same degraded performance as previous methods. In Section 5, we present stochastic (least-squares) inversion methods, using the state-variable model for the Abel transform to design Kalman filters for estimating the Abel inversion. Experimental results including comparisons with earlier methods are given.

2. ABEL INVERSION: APPLICATIONS AND METHODS

Applications of the Abel transform are diverse but unified by the circular symmetry of the phenomena being observed and the line-of-sight nature of the measurements. In studies of plasmas and flames, it is often desired to determine the radial emission profile or temperature distribution from side-on brightness observations.[3–5] Temperature profiles have also been obtained by Abel inversion of transverse interferograms[6] and Doppler information.[7] Similar brightness/emission problems occur in astronomy.[8,9] Transverse interferometry, together with Abel inversion, is used for refractive-index measurement in plasmas[10–12] and optical fibers.[13] Schlieren techniques have also been applied to refractometry.[14] The droplet distribution in an axisymmetric spray is related to scattered incident light by an Abel transform.[15] In microscopy, certain stereology models make use of Abel inversion to obtain two- and three-dimensional structural information from one-dimensional measurements.[16,17] The line-spread and point-spread functions of imaging systems are related by the Abel transform,[2] and a similar relationship exists between acoustic pressure fields from line sources and circularly symmetric planar sources.[18] The fact that the zero-order Hankel, or Fourier–Bessel, transform is the (one-dimensional) Fourier transform of an Abel transform is the basis of fast algorithms for Hankel-transform computation.[19–21] And finally, the Abel transform is of interest because it is an example of a more general approach to image reconstruction.[22]

We point out here that there are practical situations in

0740-3232/85/040510-11$02.00

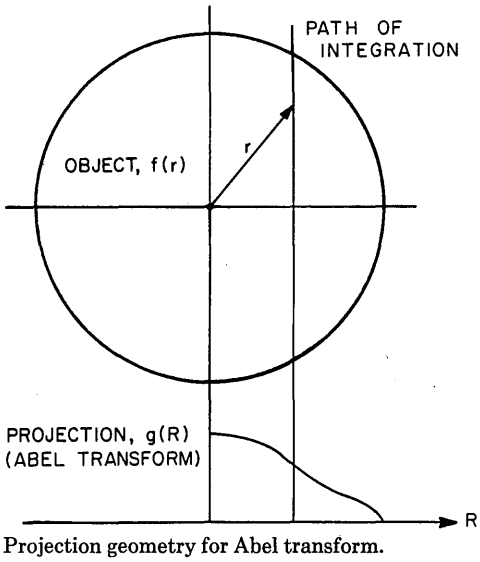

Fig. 1. Projection geometry for Abel transform.

which the Abel transform pair, Eqs. (1) and (2), does not strictly apply, and corrections must be made to the theory. These include strongly refracting plasmas[11] and cases in which emission occurs simultaneously with self-absorption.[23,24] These problems are, however, outside the scope of this paper, and in what follows we shall restrict ourselves to those cases in which Eqs. (1) and (2) are valid.

Just as there is an abundance of Abel transform applications, several methods have been used for computation. The inverse transform has received most of the attention, because the forward transform is usually implicit in a measurement situation, and the inversion is required to interpret the data. Computation of the Abel inversion, particularly in the presence of random errors in experimental data (noise), is a difficult problem. The forward transform is an integration process; inversion necessarily involves differentiation of the data [cf. Eqs. (2)], yet differentiation exacerbates the effects of noise. Several studies have shown[25–27] that inversion algorithms in which the derivative is approximated by, say, a finite difference are numerically unstable; the variance of the reconstruction error varies inversely with the sampling interval so that the more data points one takes, the worse the results will be. A further complication is that the Abel transform, while linear, is space variant (nonconvolutional); hence the efficient fast-Fourier-transform-based methods for computing convolutions do not apply, and either general numerical integration [typically requiring $O(N^2)$ multiplications] or matrix inversion [$O(N^3)$ multiplications] must be used. The Abel transforms do become convolutional on coordinate transformation (change of variable), and more will be said about this in Section 3. Finally, the Abel inversion problem is often complicated by the nonuniform spacing of the data itself, such as fringe locations in interferometry, or by the desire in spectroscopy to study the center of a plasma, near the discharge, more closely than the edges.[28] The methods presented in this paper are fast, can handle arbitrarily spaced data, and also take noise into account in a least-squares optimum sense.

The majority of published approaches to Abel inversion are based on modeling either the experimental data or the unknown radial profile as some sort of simple curve. With this assumption, the integrals in Eqs. (1) and (2) reduce to simultaneous linear algebraic equations that are then solved by standard techniques. In the earliest approach,[29] the object was divided into annuli with the assumption that it was constant in each annulus:

$$f(r) = f_n, \qquad r_n \geq r \geq r_{n-1}.$$

The forward Abel transform is obtained by direct integration of this piecewise constant model, resulting in a set of linear algebraic equations in the unknown annulus values:

$$\sum_{n=1}^{N} a_n f_n = g_n.$$

Given experimental data $\{g_n\}$, this set of equations is solved for the annulus values $\{f_n\}$. A second early approach[30,31] attacked the inverse-transform integral directly, approximating the data by a piecewise low-order polynomial fit and computing the derivative by differentiating the polynomials. The integral was then discretized to a summation by standard numerical means. The fit was exact, so that noise in the data was reproduced exactly; as we said earlier, this approach is prone to large errors. Barr[28] improved on this approach by using Eq. (2b) and smoothing the integral before applying the derivative.

Several authors have tackled the noise problem by fitting smooth curves to larger portions of the data, thus implicitly filtering out the noise. The data are divided into several zones, each containing several points; using least-squares methods, the expansion is then made

$$g(R) = \sum_{n=1}^{N} a_n \phi_n(R),$$

where the functions $\{\phi_n(R)\}$ have known or easily calculated Abel inversions $\{\theta_n(r)\}$. The reconstruction $f(r)$ is then given by

$$f(r) = \sum_{n=1}^{N} a_n \theta_n(r).$$

The popular method of Cremers and Birkebak[32] employed a piecewise fit of fourth-order polynomials. Their paper also provides a comparison of several early algorithms. Minerbo and Levy[25] used instead an expansion of the entire data set in orthogonal polynomials; their paper also provides helpful comparisons. While they used Hermite polynomials, other orthogonal sets have been proposed, including (trigonometric) Fourier series,[33] Fourier–Bessel series and Zernike polynomials,[34] and Legendre polynomials.[35] In recent years, spline fits to the data have been studied,[27,36,37] and these also offer significant improvement over the Nestor–Olsen family of methods.

We also mention that it is possible to model the object in terms of basis functions with unknown expansion coefficients (in its simplest form, this is the early piecewise-constant annulus model):

$$f(r) = \sum_{n=1}^{N} b_n \theta_n(r).$$

Again assuming that the Abel transforms of the functions $\{\theta_n(r)\}$ are known, we have

$$g(R) = \sum_{n=1}^{N} b_n \phi_n(R).$$

Given a set of experimental data, this relation becomes a set

of simultaneous linear algebraic equations in the unknown expansion coefficients $\{b_n\}$. Once solved, the object is reconstructed from the $\{b_n\}$ and $\{\theta_n(r)\}$. The use of piecewise linear models has been reported.[38,39] An interesting extension of this concept is the use of the finite-element method.[40] The object is modeled as piecewise linear; the nodal values of these linear finite elements are chosen to minimize the mean-square difference between the experimental data and the forward Abel transform of the finite-element model. The result is a set of simultaneous linear algebraic equations in the unknown nodal values.

In a departure from these direct least-squares curve fits, Anderssen took a Wiener filtering approach to the differentiation of the data.[26] Viewed in the frequency domain, the derivative operator corresponds to a filter with magnitude response proportional to frequency. High frequencies are increasingly weighted with respect to low frequencies, with the result that the noise, which tends to have more high-frequency content than the signal, is emphasized over the signal. In Anderssen's spectral differentiation method, the derivative is performed by a digital filter that, according to the Wiener least-squares criterion, rolls off in the frequency domain when the signal-to-noise ratio becomes too low. This provides an optimal least-squares estimate of the derivative. The integration is then done numerically. This method was applied to Abel inversion using both Eqs. (2a) and (2b) and is compared with the Minerbo and Levy method in Ref. 26. The method developed in this paper is compared with these approaches in Section 5.

3. STATE-VARIABLE MODELING OF THE ABEL TRANSFORM

The Abel transforms are linear, space-variant operators; as such, they are not convolutions, and the efficient computational methods (i.e., using the fast Fourier transform) that have been devised for space-invariant systems cannot be used. However, they become space invariant (convolutional) under appropriate coordinate transformations (changes of variable). After such a transformation is performed, space-invariant processing may be done in the new coordinate space; an inverse coordinate transformation returns the result to the original domain. This method is well known in optics, having been applied to image restoration[41,42] and pattern recognition.[43] It has also been applied to the Abel transform.[1,44–46] These methods have the disadvantage that either the data must be taken on a nonuniform grid, which is not possible in the case of interferometry, for example, or else they must be interpolated to a nonuniform grid. Interpolation imposes its own computational burden, offsetting the advantages of space invariance. It may also be sensitive to noise and usually requires that the number of interpolated data points be greater than the original number to satisfy the sampling theorem in the transformed coordinate system.[47,48] Our method makes use of coordinate transformation, but we avoid the drawbacks by using it solely to model the Abel transform and derive the reconstruction filters. The resulting filters are *space variant* and require *no* coordinate transformation of the data.

The approach taken is to treat the Abel transform as a system modeled by a set of linear differential equations—in this framework, the Abel transform $g(R)$ is the solution of a differential equation with $f(r)$ as its driving function. Likewise, the Abel inversion $f(r)$ may be computed as the solution of a differential equation with $g'(R)$ as its driving function.

The differential equations that we derive are of the state-variable type. State-variable methods are well known in control theory and comprise a powerful and general approach to the analysis and design of linear systems.[49] The standard linear state-variable model for a time-domain system is

$$x'(t) = A(t)x(t) + B(t)u(t),$$
$$y(t) = C(t)x(t) + D(t)u(t).$$

It consists of a first-order matrix differential equation and a linear matrix algebraic equation. The input is $u(t)$, and the output is $y(t)$. The vector $x(t)$ is called the system-state vector, and its components are called state variables; the matrices $\{A, B, C, D\}$ are of dimensions appropriate to the numbers of inputs, outputs, and state variables. The state vector is updated in time by the system's internal dynamics (represented by the matrix A) and the input $u(t)$ (by B). The output $y(t)$ is formed as a linear combination of the state variables (by C) and, occasionally, direct feedthrough of the input (by D). The model is general, accommodating systems with multiple inputs and outputs and time-varying parameters. In the simple case of a system with a single input and output, B and C become column and row vectors, respectively, and D reduces to a scalar. Furthermore, if the system is time invariant, the parameters $\{A, B, C, D\}$ are constant.

The parameters $\{A, B, C, D\}$ completely characterize the system dynamics and are said to comprise a *realization* of the system's impulse response. In the time-invariant case, the impulse response is related to the parameters by

$$h(t) = C \exp(At)B; \tag{3}$$

computation of the impulse response for a time-varying system is considerably more complicated.[50]

The modeling procedure that we follow is diagrammed in Fig. 2. A time- or space-variant superposition integral is transformed to a convolution by the application of a suitable coordinate transformation. The constant parameters $\{\tilde{A}, \tilde{B}, \tilde{C}\}$ (assuming no direct feedthrough, D) are chosen to realize the impulse response of the transformed system. Applying the inverse coordinate transformation *to the state equations*

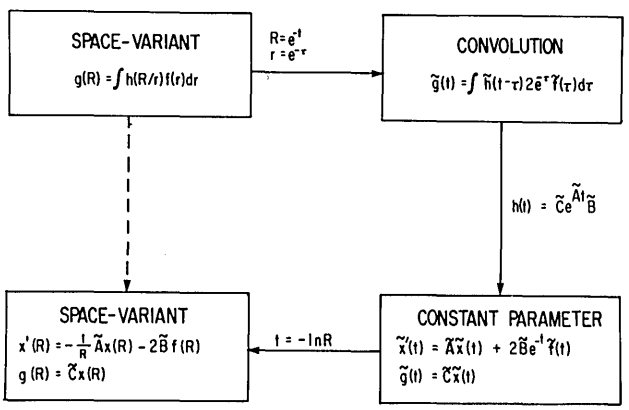

Fig. 2. Steps in state-variable modeling by coordinate transformation. The space-variant superposition integral is converted to a convolution by a coordinate transformation. The convolution is realized by an equivalent set of constant-parameter state equations. Finally, the inverse coordinate transformation is applied to the state equations, yielding a set of space-variant state equations equivalent to the original superposition integral.

Table 1. Parameters of Exponential Approximation to Abel Transform Impulse Response

j	h_j	λ_j
1	0.318	0
2	0.19	−2.1
3	0.35	−6.2
4	0.82	−22.4
5	1.8	−92.5
6	3.9	−414.5
7	8.3	−1889.4
8	19.6	−8990.9
9	48.3	−47391.1

results in a set of equations with nonconstant parameters that models the original space-variant system. In this way, the coordinate transformation makes the otherwise difficult space-variant modeling problem tractable. A general discussion of the method for arbitrary systems and transformations has been presented elsewhere.[51]

To apply this procedure to the Abel transform, Eq. (1), we first rewrite it in the form

$$g(R) = \int_0^\infty f(r) \frac{2U(1 - R/r)}{[1 - (R/r)^2]^{1/2}} \mathrm{d}r, \tag{4}$$

where $U(\cdot)$ is the unit step function. Applying the coordinate transformation $R = \exp(-t)$, $r = \exp(-\tau)$ results in

$$\tilde{g}(t) = \int_{-\infty}^{\infty} 2 \exp(-\tau) \tilde{f}(\tau) \frac{U(t - \tau)}{\{1 - \exp[-2(t - \tau)]\}^{1/2}} \mathrm{d}\tau, \tag{5}$$

where $\tilde{g}(t) = g[\exp(-t)]$, etc. This is the convolution of a modified input $2 \exp(-t)\tilde{f}(t)$ with a space-invariant impulse response $\tilde{h}(t) = [1 - \exp(-2t)]^{-1/2} U(t)$. Constant-parameter state equations follow directly:

$$\begin{aligned} \tilde{x}'(t) &= \tilde{A}\tilde{x}(t) + 2\tilde{B} \exp(-t)\tilde{f}(t), \\ \tilde{g}(t) &= \tilde{C}\tilde{x}(t), \end{aligned} \tag{6}$$

where $\{\tilde{A}, \tilde{B}, \tilde{C}\}$ realize $\tilde{h}(t)$:

$$\tilde{h}(t) = \tilde{C} \exp(\tilde{A}t)\tilde{B} = [1 - \exp(-2t)]^{-1/2}, \qquad t \geq 0. \tag{7}$$

It is convenient to choose a diagonal form for $\tilde{A}$, viz.,

$$\begin{aligned} \tilde{A} &= \mathrm{diag}[\lambda_1, \lambda_2, \ldots, \lambda_K], \\ \tilde{B} &= [h_1 h_2 \ldots h_K]^T, \\ \tilde{C} &= [1\,1 \ldots 1], \end{aligned} \tag{8}$$

from which it follows that

$$\tilde{C} \exp(\tilde{A}t)\tilde{B} = \sum_{k=1}^{K} h_k \exp(\lambda_k t) = [1 - \exp(-2t)]^{-1/2}, \qquad t \geq 0. \tag{9}$$

The eigenvalues $\{\lambda_k\}$ and expansion coefficients $\{h_k\}$ were found by the following least-squares method.[52] The impulse response $\tilde{h}(t)$ is monotonically decreasing, so it is reasonable that a decomposition in pure decaying exponentials (real, negative eigenvalues) may be made. Taking the logarithm of the impulse response, a straight line fit was made to the tail of the curve ($t \gg 0$) under the assumption that all the exponentials except one had died out by that point. The slope and the y intercept of this line gave the eigenvalue and the coefficient, respectively, of an exponential approximation to the tail of the impulse response. This exponential was then subtracted from the impulse response, and the process was repeated until a satisfactory model was achieved. Using this technique, a ninth-order model with an rms error of 0.001 was found, having the parameters shown in Table 1. More-automatic system-identification techniques have been tried, but none have so far bested this first attempt.

Applying the inverse coordinate transformation $t = -\ln R$ to the state equations results in

$$\begin{aligned} x'(R) &= -\frac{1}{R}\tilde{A}x(R) - 2\tilde{B}f(R), \\ g(R) &= \tilde{C}x(R). \end{aligned} \tag{10}$$

Note that the matrix $A(R) = -\tilde{A}/R$ is a constant matrix multiplied by a scalar function of R. This holds in general for this class of space-variant model[51,53] and makes for efficient updating in numerical solutions.

Derivation of a model for Abel inversion, Eq. (2a), parallels that of the forward transform. The resulting state-variable equations are

$$\begin{aligned} x'(r) &= -\frac{1}{r}\tilde{A}x(r) + \frac{1}{\pi r}\tilde{B}q'(r), \\ f(r) &= \tilde{C}x(r), \end{aligned} \tag{11}$$

where, again,

$$\tilde{C} \exp(\tilde{A}t)\tilde{B} = [1 - \exp(-2t)]^{-1/2}, \qquad t \geq 0. \tag{12}$$

The forward and inverse models in Eqs. (10) and (11) are quite similar, and the same $\{\tilde{A}, \tilde{B}, \tilde{C}\}$ may be used for both.

The initial conditions for these equations are given by the values of $f(r)$ and $g(R)$ at their outer edges (for the forward and inverse transforms, respectively). The outputs are then computed recursively *inward* to the origin; recursion accounts for the efficiency of these algorithms relative to other, batch methods.

The state equations may be simulated by standard numerical techniques (trapezoid, Runge–Kutta, etc.), or they may be converted to space-variant linear difference equations. The latter follow from the explicit solution of the state equation, which is known to be[54]

$$x(R) = \Phi(R, R_0)x(R_0) + 2\int_{R_0}^{R} \Phi(R, r)\tilde{B}f(r)\mathrm{d}r. \tag{13}$$

The first term of the right-hand side is the homogeneous, or undriven, part, while the superposition integral represents the steady-state, or driven, solution. The key quantity is the state-transition matrix $\Phi(R, R_0)$, which, for this class of systems, is found to be[51,55]

$$\begin{aligned} \Phi(R, R_0) &= \exp[\tilde{A} \ln(R_0/R)] \\ &= \mathrm{diag}[(R_0/R)^{\lambda_1}, \ldots, (R_0/R)^{\lambda_K}]. \end{aligned} \tag{14}$$

We discretize this solution by letting $R_0 = (N - n)\Delta$, $R = (N - n - 1)\Delta$, where N is the number of data points and Δ is the sampling interval [$=R_{\max}/(N - 1)$]; $f(r)$ is assumed constant on (R_0, R) (staircase or zero-order hold approximation). The assumption of a uniform sampling grid is not necessary, as the procedure easily accommodates nonuniformly spaced samples. We obtain, for the forward Abel transform,

$$\left.\begin{aligned} x_{n+1} &= \Phi_n x_n + \Gamma_n f_n \\ g_n &= \tilde{C} x_n \end{aligned}\right\} \qquad n = 0, \ldots, N-1, \tag{15}$$

where

$$x_n = x[(N-n)\Delta], \text{ etc.},$$

$$\Phi_n = \Phi[(N-n-1)\Delta, (N-n)\Delta]$$

$$= \operatorname{diag}\left[\left(\frac{N-n}{N-n-1}\right)^{\lambda_1}, \ldots, \left(\frac{N-n}{N-n-1}\right)^{\lambda_K}\right], \tag{16a}$$

$$\Gamma_n = [h_1\gamma_n(\lambda_1), \ldots, h_K\gamma_n(\lambda_K)]^T, \tag{16b}$$

and

$$\gamma_n(\lambda) = \frac{2(N-n-1)\Delta}{\lambda+1}\left(1 - \left(\frac{N-n}{N-n-1}\right)^{\lambda+1}\right), \quad \lambda \neq -1. \tag{16c}$$

For the inverse Abel transform, we obtain a similar, though not identical, result:

$$\left.\begin{aligned} x_{n+1} &= \Phi_n x_n + \Gamma_n g'_n, \\ f_n &= \tilde{C} x_n, \end{aligned}\right\} \qquad n = 0, \ldots, N-2, \tag{17}$$

where Φ_n and Γ_n are as in Eqs. (14a) and (14b) but $\gamma_n(\lambda)$ is given by

$$\gamma_n(\lambda) = \begin{cases} -\dfrac{1}{\pi}\ln\left(\dfrac{N-n}{N-n-1}\right), & \lambda = 0 \\ \dfrac{1}{\pi\lambda}\left(1 - \left(\dfrac{N-n}{N-n-1}\right)^{\lambda}\right), & \lambda \neq 0 \end{cases}. \tag{18}$$

The recursions proceed from the outer edge of the object or projection toward the origin, i.e., when $n = 0$, $R = R_{\max}$, and when $n = N-1$, $R = 0$; in the case of Abel inversion, the recursion actually stops at $n = N-2$, since $\gamma_{N-1}(0) = \infty$.[56] The recursive, diagonalized structure of the filter has the result that, for N data points and K state variables, only $2KN$ multiples are required to compute g from f or vice versa, in contrast to a computational burden of $O(N^2)$ for numerical integration. For $N > 2K$, this amounts to a considerable improvement in computational speed over previous methods.

4. DETERMINISTIC ABEL INVERSION

The Abel inversion given by Eqs. (15)–(18) is a direct realization of the inverse integral in Eq. (2a); hence we shall refer to it as the deterministic filter. The derivative sequence $g'_n = g'[(N-n)\Delta]$ is computed (by a forward difference, say) and used to drive the state-variable model. In Fig. 3, we show the results of a simulation using the known Abel transform pair A given in Table 2. The mean-square error (MSE) is quite low, 1.33×10^{-6}, a result that was duplicated for several other test functions.[51]

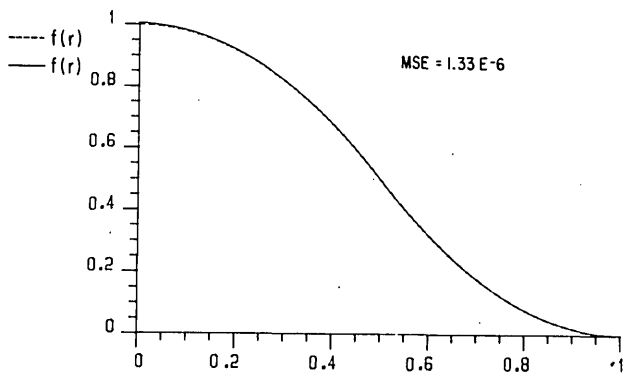

Fig. 3. Deterministic inversion of noiseless projection data, curve A, $N = 101$; dashed and solid lines are true and computed curves, respectively. Mean-squared error (MSE) = 1.33×10^{-6}.

Table 2. Test Functions Used in Simulations

Curve A

$$f(r) = \begin{cases} 1 - 2r^2, & 0 \leq r \leq 0.5 \\ 2(1-r)^2, & 0.5 \leq r \leq 1.0 \end{cases}$$

$$g(R) = \begin{cases} \dfrac{2}{3}[2\alpha(1+2R^2) - \beta(1+8R^2)] - 4R^2\ln\left(\dfrac{1+\alpha}{0.5+\beta}\right), & 0 \leq R \leq 0.5 \\ \dfrac{4}{3}\alpha(1+2R^2) - 4R^2\ln\left(\dfrac{1+\alpha}{R}\right), & 0.5 \leq R \leq 1.0 \end{cases}$$

where

$$\alpha = (1-R^2)^{1/2}, \qquad \beta = (0.25 - R^2)^{1/2}$$

Curve B

$$f(r) = (1-r^2)^{-3/2} \times \exp\left[\frac{(1.1r)^2}{r^2-1}\right]$$

$$g(R) = \frac{\pi^{1/2}}{1.1}(1-R^2)^{-1/2} \times \exp\left[\frac{(1.1R)^2}{R^2-1}\right]$$

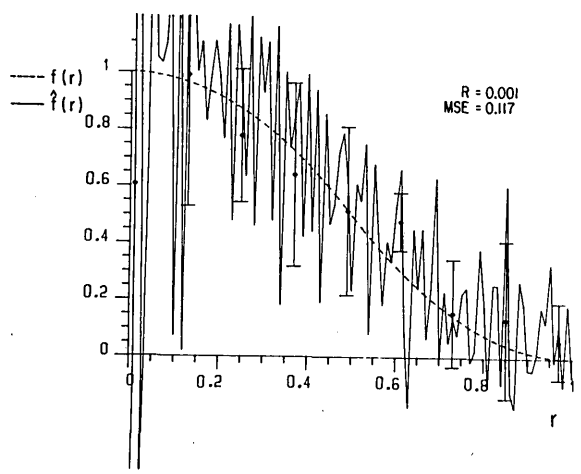

Fig. 4. Deterministic inversion of noisy projection data, curve A, $N = 101$, noise variance $R = 0.001$; dashed and solid lines are true and computed curves, respectively.

Figure 4 shows the attempted deterministic reconstruction of the same curve A but with the projection g_n corrupted by a modest amount of white Gaussian noise. The noisy data are denoted z, where $z_n = g_n + v_n$, and the noise v_n has zero mean and a variance of 0.001. The reconstruction is unacceptable, which may be attributed to the differentiation of the projection. The forward-difference approximation to the derivative acts on the white-noise sequence v_n to produce a new noise sequence whose variance is inversely proportional to the square of the step size—in other words, while one usually expects more data to give better results, here the signal-to-noise ratio actually decreases as more data are taken.

5. LEAST-SQUARES ABEL INVERSION

A. Kalman Filter Design

When the projection $g(R)$ is noisy, the deterministic inverse filter fails. It is therefore natural to seek an inversion procedure that takes the noise into account, i.e., a filter that produces an optimum estimate of $f(r)$ relative to some criterion. The most well-known class of estimator is based on a least-squares criterion, minimizing the variance of the estimation error. This idea, applied to a signal model in state-variable form, results in the Kalman filter.[58] Originally applied to tracking and control problems, the Kalman filter has also been applied to seismic deconvolution[59] and image restoration.[60–62]

Given a state-variable model

$$x_{n+1} = F_n x_n + G_n w_n,$$

$$z_n = H_n x_n + v_n,$$

where w and v are assumed to be zero mean, white, and Gaussian, the Kalman filter produces the best linear least-squares estimate of the state vector x. The process w_n is called the process noise and is thought of as driving the signal model. The process v_n is called the sensor or measurement noise. The noises need not be stationary, nor does the signal model need to be time invariant for the Kalman filter to be applied; of course, significant simplifications result if these conditions are met.

We shall return later to the precise form of the Kalman filter equations. First, we develop a stochastic signal model for the (forward) Abel transform. The discrete system $\{\Phi_n, \Gamma_n, \tilde{C}\}$ in Eqs. (15) and (16) models the projection of an object $f(r)$ into the Abel transform $g(R)$. To complete the picture, we need a statistical characterization of the object $f(r)$. The simplest possible model, apart from just assuming that f is pure white noise, is to assume a recursive form in which the next value of f is equal to the current value plus some increment that is unknown *a priori*. Taking this increment to be white and Gaussian, we have

$$f_{n+1} = f_n + w_n.$$

The process noise w_n is also assumed here to be zero mean and stationary, with covariance

$$E\{w_n w_m\} = Q\delta_{nm}$$

where δ_{nm} is the Kronecker delta function.

This model for f_n is combined with the forward Abel model in Eqs. (15) and (16) by taking f_n as an additional state variable. Let an augmented state vector ξ_n be defined:

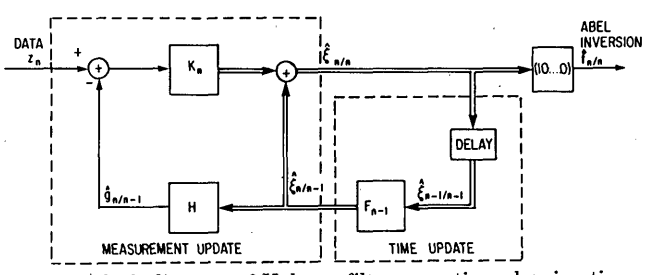

Fig. 5. Block diagram of Kalman filter operation, showing time-update (prediction) and measurement-update (correction) steps.

$$\xi_n = \begin{bmatrix} f_n \\ x_n \end{bmatrix}.$$

With this, the augmented state equations are found to be

$$\xi_{n+1} = F_n \xi_n + G w_n,$$

$$z_n = g_n + v_n = H\xi_n + v_n, \tag{19}$$

where

$$F_n = \left[\begin{array}{c|c} 1 & 0 \ldots 0 \\ \hline \Gamma_n & \Phi_n \end{array}\right],$$

$$G = [1|0 \ldots 0]^T,$$

$$H = [0|\tilde{C}]. \tag{20}$$

The sensor or measurement noise v_n is assumed zero mean, white, Gaussian, and stationary, independent of w_n, with covariance[63]

$$E\{v_n v_m\} = R\delta_{nm}.$$

The Kalman filter produces its estimates of the state vector ξ_n in two stages (Fig. 5). First, assume that at time $n-1$, an estimate exists that is based on all previous and current data $\{z_1, \ldots, z_{n-1}\}$. This estimate is denoted $\hat{\xi}_{n-1/n-1}$ and is called the filtered estimate. Associated with the estimate is an estimation error, characterized by the covariance matrix

$$\Sigma_{n-1/n-1} = E\{(\xi_{n-1} - \hat{\xi}_{n-1/n-1})(\xi_{n-1} - \hat{\xi}_{n-1/n-1})^T\}.$$

In the *time-update* step, the next state is *predicted* by the signal model without using any new data; this update obeys the equations

$$\hat{\xi}_{n/n-1} = F_{n-1}\hat{\xi}_{n-1/n-1}, \tag{21a}$$

$$\Sigma_{n/n-1} = F_{n-1}\Sigma_{n-1/n-1}F_{n-1}{}^T + GQG^T. \tag{21b}$$

The predicted output $\hat{g}_{n/n-1} = H\hat{\xi}_{n/n-1}$ is the model's estimate of what the next data point should be. In the *measurement-update* step, this predicted data point is compared with the actual data z_n, and an error signal is generated (this is also known as the *innovations process*, since it bears the new, or innovative, information content of the data relative to the model's predictions):

$$\tilde{z}_{n/n-1} = z_n - H\hat{\xi}_{n/n-1}. \tag{21c}$$

The innovations are blended with the predicted estimate to produce a new filtered estimate, according to

$$\hat{\xi}_{n/n} = \hat{\xi}_{n/n-1} + K_n\tilde{z}_{n/n-1}, \tag{21d}$$

$$\Sigma_{n/n} = \Sigma_{n/n-1} - K_n H\Sigma_{n/n-1}. \tag{21e}$$

The desired object estimate is the first component of this state estimate:

$$\hat{f}_{n/n} = [1|0 \ldots 0]\hat{\xi}_{n/n}. \tag{21f}$$

The key quantity is the *Kalman gain* K_n. It is computed from the equation

$$K_n = \Sigma_{n/n-1}H^T(H\Sigma_{n/n-1}H^T + R)^{-1}. \tag{21g}$$

The Kalman gain is a function of the signal model by the state-prediction error covariance $\Sigma_{n/n-1}$ and the quantity $H\Sigma_{n/n-1}H^T + R$, which may be shown to be the innovations variance.[64]

Two initial conditions are required to start the recursions:

the initial state $\hat{\xi}_{0/0}$ and the covariance $\Sigma_{0/0}$. The values used in our simulations are

$$\Sigma_{0/0} = GQG^T$$
$$\hat{\xi}_{0/0} = [0|0 \ldots 0]^T. \tag{21h}$$

One also needs values for R and Q, the measurement and process noise variances. The measurement noise variance is assumed known, as it may usually be obtained in practice by measurement of noise power in the detector. Arriving at a value for the process noise variance is more difficult, since it is not only a measure of the signal power but also is typically used to compensate for errors in the signal model. In general, if the process noise is much lower than the measurement noise, then the Kalman filter will trust the predictions of the signal model (by the time update) over the observed data. Similarly, if the process noise is much higher than the measurement noise, the filter will rely heavily on the observed data to correct the predictions of the model. The simple first-order signal model assumed here is not expected to portray the true object $f(r)$ accurately; the Kalman filter is informed of this by the process noise variance Q.

In our simulations, we arrived at an initial value for the process noise variance by the following method.[65] From the signal model, Eq. (19), we may obtain an expression for the data variance

$$\mathrm{Var}(z_n) = H\Sigma_n H^T + R, \tag{22}$$

where Σ_n is the covariance of the model's state vector. It is convenient to normalize this covariance matrix by the (scalar) process noise variance Q; the normalized matrix may be shown to obey the recursion

$$\frac{\Sigma_{n+1}}{Q} = F_n \frac{\Sigma_n}{Q} F_n^T + GG^T. \tag{23}$$

From Eq. (23), we recursively compute the normalized covariance sequence for $n = 1, 2, \ldots, N$, beginning with $\Sigma_0/Q = GG^T$. We average the normalized covariance matrix over all n and derive an average data variance σ_z^2:

$$\sigma_z^2 = \bar{P}Q + R, \tag{24}$$

where

$$\bar{P} = H(\bar{\Sigma}/Q)H^T. \tag{25}$$

The average signal variance $\bar{P}$ is completely data independent, in that the unknown process noise variance has been normalized out, and so it may be computed once for a particular signal model and applied to any data set assumed to satisfy that model. The only on-line (data-dependent) step is actually to compute the variance σ_z^2, with which we then estimate Q from Eq. (25) by

$$Q_{\mathrm{estim}} = \frac{\sigma_z^2 - R}{\bar{P}}. \tag{26}$$

In practice, this estimate of Q was found to be a satisfactory rough estimate, but the best results were obtained when it was replaced by a weighted version:

$$Q = \begin{cases} 10(RQ_{\mathrm{estim}})^{1/2}, & R > 10^{-5} \\ 0.025Q_{\mathrm{estim}}, & R < 10^{-5} \end{cases}. \tag{27}$$

These weighted Q values were used in the simulations of the following section. More-sophisticated methods might try to correct modeling errors by using higher-order Gauss–Markov signal models and/or segmenting the data and computing different Q's for successive zones.

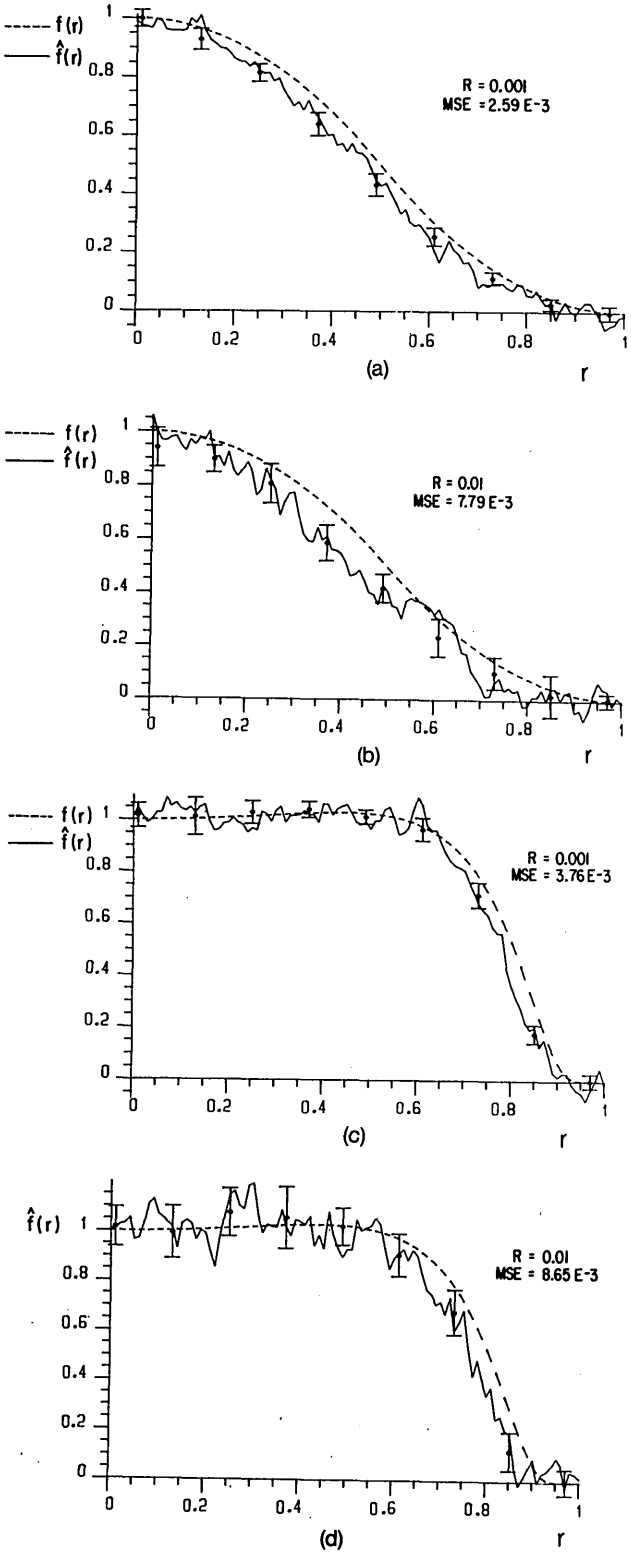

Fig. 6. Kalman filter inversion of noisy projection data. (a) Curve A, $R = 0.001$. (b) Curve A, $R = 0.01$. (c) Curve B, $R = 0.001$. (d) Curve B, $R = 0.01$. Dashed and solid lines are true and computed curves, respectively; error bars are ± one standard deviation about ensemble mean of 12 runs.

B. Experimental Results

Figure 6 shows four examples of Abel inversion from noisy data using the Kalman filter. The functions are curves A and B, shown in Table 2. Two measurement-noise variances are considered, $R = 0.01$ and $R = 0.001$. The error bars are computed relative to an ensemble of 12 runs with independent noise sequences; the bars display one standard deviation above and below the ensemble average. The mean-square errors are acceptably low, especially as compared with the deterministic inverse (Fig. 4). We do observe, however, that the estimates tend to be biased below the true (dashed) curves. This is an artifact of the signal model in the time-update step, which predicts the next value of $\hat{f}$ to be the same as the current value. Since the curves are generally increasing inward, this prediction will tend to be low. (By contrast, note that the reconstruction of curve B is nearly unbiased in the flatter region near the origin. In nonmonotonic test functions, the estimates of decreasing segments are, predictably, biased high.[57]) By increasing the process noise variance, the bias can be decreased at the cost of higher variance in the reconstruction. In effect, the Q that we used was judged to give the best compromise between bias and variance. The smoothing filters, to be discussed next, are also effective at removing bias.

C. Inversion with Smoothing

The Kalman filter described above recursively computes the Abel inversion beginning at the outer edge of the object and working inward. We have found that better reconstructions are obtained by performing a second pass over the data to smooth the estimates. There are several types of optimal smoothing filters[66]; we employed the *fixed-interval smoother*, which is particularly well suited to this problem.

The fixed-interval smoother makes use of the entire data set in computing each point in the reconstruction. Contrast this with the Kalman filter estimate above, in which $\hat{f}_1$ is computed solely from z_1, $\hat{f}_2$ from z_1 and z_2, and so on, until $\hat{f}_N$ is computed from z_1 through z_N. The smoother operates by taking the *predicted* estimates from the Kalman filtering step and making a second sweep backward through the data set from N to 1. Because more data are employed in computing the smoothed estimate than in the filtered estimate, the smoothed estimate is generally more accurate. This comes at a cost of about 20% more computation.

Our smoothing procedure is based on the modified Bryson–Fraser (MBF) algorithm.[67] It uses the Kalman gains K_n and innovations $\tilde{z}_{n/n-1}$ from the first (Kalman filter) pass to construct the smoothed estimate $\hat{\xi}_{n/N}$ and the associated covariance $\Sigma_{n/N}$. The algorithm is simplified in our case, since we are interested in smoothing only the first component of $\hat{\xi}$ (i.e., $\hat{f}$) and choose to neglect the covariance $\Sigma_{n/N}$.

The MBF algorithm recursively generates a (vector) quantity $S_{n/N}$ by

$$S_{n/N} = Y_{n+1/n}^T S_{n+1/N} + H^T[H\Sigma_{n/n-1}H^T + R]^{-1}\tilde{z}_{n/n-1}, \quad n = N, N-1, \ldots, 1, \tag{28a}$$

where

$$Y_{n+1/n} = F_n[I - K_nH], \tag{28b}$$

$$\tilde{z}_{n/n-1} = z_n - H\hat{\xi}_{n/n-1}, \tag{28c}$$

and

$$S_{N+1/N} = [0 \ldots 0]^T. \tag{28d}$$

The smoothed estimates $\hat{\xi}_{n/N}$ are then computed by

$$\hat{\xi}_{n/N} = \hat{\xi}_{n/n-1} + \Sigma_{n/n-1}S_{n/N}.$$

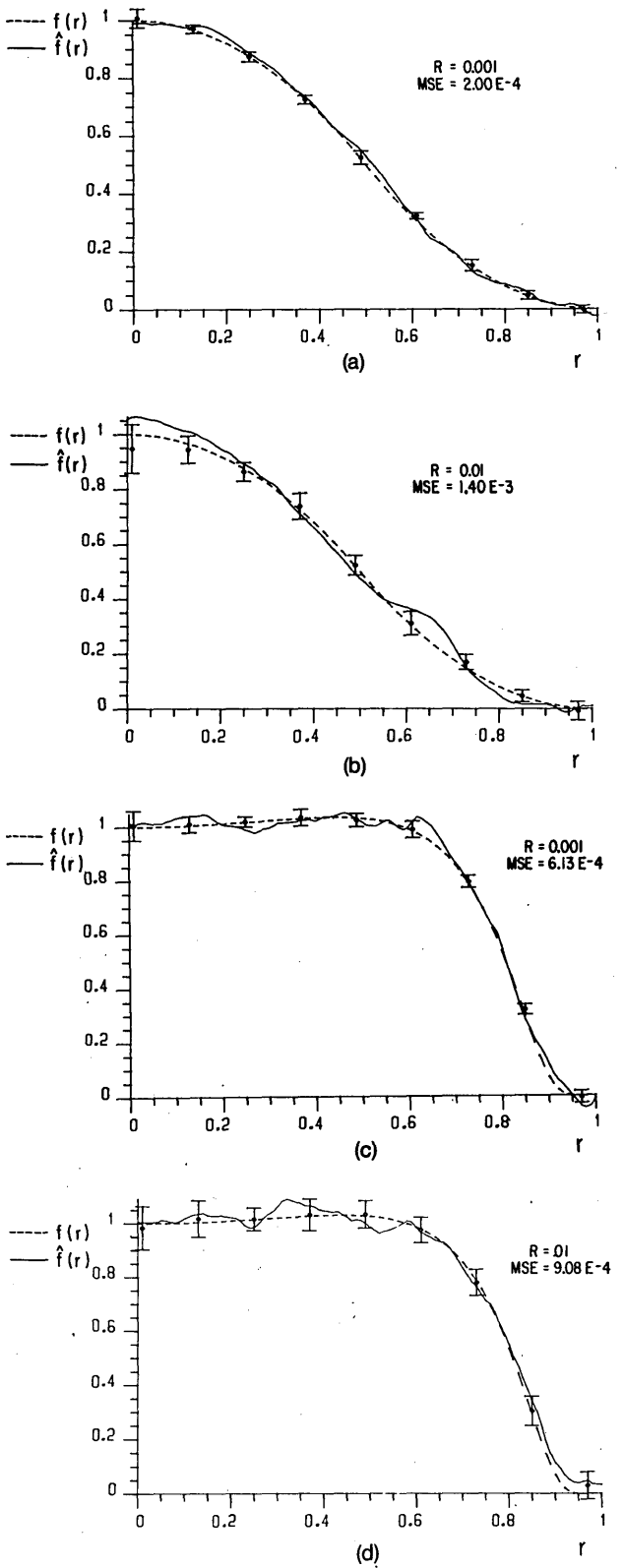

Fig. 7. Fixed-interval smoothing applied to Kalman filter inversions. Same data as Fig. 6.

Since we require only the first component of the state vector ξ, the equation simplifies to

$$\hat{f}_{n/N} = \hat{f}_{n/n-1} + [1\,0\ldots0]\Sigma_{n/n-1}S_{n/N}, \quad n = N, N-1, \ldots, 1. \quad (28e)$$

The quantity $[1\,0\ldots0]\Sigma_{n/n-1}$ is the first row of the covariance matrix. Close examination of Eq. (28a) reveals that $S_{n/N}$ is a combination of the innovations $\{\tilde{z}_{N/N-1}, \tilde{z}_{N-1/N-2}, \ldots, \tilde{z}_{n/n-1}\}$; hence it contains the data $\{z_n, z_{n+1}, \ldots, z_N\}$. The predicted estimates in Eq. (28e) are based on the data $\{z_1, z_2, \ldots, z_{n-1}\}$. Thus we see that the smoothed estimate does indeed contain all the data points $\{z_1, z_2, \ldots, z_N\}$.

Smoothed Abel inversions are shown in Fig. 7 using the same data as the Kalman filter runs (Fig. 6). Smoothing has considerably reduced the bias and the variance of the estimates, and in simulations with fewer data points ($N = 32$), the smoother had an even greater effect. Because the smoothed inversions are superior to the filtered estimates and involve only slightly more computation, we shall use them later in the comparisons with those of Minerbo and Levy and of Anderssen.

D. Computational Aspects

The Kalman filter/smoother equations (21)–(28) may appear formidable at first glance, but they are straightforward to implement. Kalman filter subroutines are available in some commercial software packages (e.g., IMSL), but we have found that there are several special features of this application that permit considerable simplification over general Kalman filter programs. This is especially important if a microcomputer is to be used. In writing programs to implement these inversion algorithms, the following points should be kept in mind: (1) The matrix F_n is quite sparse, and multiplying a vector with it takes only 2K multiply/adds. Its elements may be precomputed and stored before any data are processed. (2) The vectors G and H are composed of ones and zeros; hence operations with them may be done entirely with additions, and they require no storage. (3) The covariance matrices and the Kalman gain are determined by the signal model, not by the specific data being filtered; hence, if the variances R and Q are known *a priori* (from experience or earlier measurements, for example), then the Kalman gains for an entire run may be precomputed and stored before the run is made. Our experience has been that, while the value of Q definitely affects the quality of the reconstruction, it may vary slightly (within an order of magnitude, say) without seriously degrading performance. We have also found that overestimating R by an order of magnitude does not seriously affect the results in many cases. Hence it may not be necessary in practice to compute Q for every data set in a series of similar measurements, thus allowing the Kalman gains to be precomputed. (4) The innovations covariance $H\Sigma_{n/n-1}H^T + R$ is a scalar; hence its inverse is simply a division operation. (5) The smoother makes use of several quantities left over from the Kalman filter step, which need not be recomputed: the innovations, covariances, and Kalman gains. (6) Only the first element of the state vector, which is $\hat{f}$, is smoothed, reducing both computation and storage for the smoothing step.

Tracing through Eqs. (21) and (28), we estimate that the state equations (21a), (21c), and (21d) take $3KN$ floating-point multiplications, the covariance/gain updates [Eqs. (21b), (21e), and (21g)] just over $5K^2N$ multiplications, and the fixed-interval smoother in Eq. (28) just over K^2N multiplications, where K is the order of the state-variable model and N is the number of data points. In our simulations, $K = 9$ and $N = 101$, so the Kalman estimators are essentially $O(N^2)$. We also estimate that about 4000 floating-point memory locations are sufficient to store all the matrices and vectors for a 101-point run with smoothing.

E. Comparison with Other Methods

We compared our inversion procedures (deterministic and smoothed Kalman) with the methods of Minerbo and Levy and of Anderssen, using the test functions (curves A and B, Table 3) and data presented in Ref. 26. Throughout, $N = 101$ points are reconstructed, and three measurement-noise variances were considered in the noisy data tests: 8.3521×10^{-6}, 0.0001, 0.01. The results are shown in Table 3. [Anderssen's methods I and II are based on Eqs. (2a) and (2b), respectively.] The notation $\sigma(f; m, n)$ denotes the standard deviation of the error $f - \hat{f}$, measured over the interval $[m, n]$;

Table 3. Comparison of Deterministic and Kalman Filter/Smoother Reconstructions with Minerbo–Levy (M-L) and Anderssen (A-I and A-II) Methods

	Curve A				Curve B			
Noiseless Data	Deterministic	M-L	A-I	A-II	Deterministic	M-L	A-I	A-II
$\sigma(f; 1, 101)$	1.09E-3	3.15E-3	8.88E-4	5.63E-3	1.62E-3	1.45E-2	1.68E-4	1.29E-2
$\sigma(f; 6, 96)$	8.43E-4	2.58E-3	3.23E-4	1.08E-4	1.68E-3	1.02E-2	1.67E-4	2.20E-4
$\sigma(f; 11, 91)$	8.37E-4	2.62E-3	2.83E-4	9.84E-5	1.72E-3	9.99E-3	1.39E-4	1.59E-4
Noisy Data	Kalman Filter	M-L	A-I	A-II	Kalman Filter	M-L	A-I	A-II
$R = 8.3521E\text{-}6$								
$\sigma(f; 1, 101)$	7.51E-3	4.50E-3	9.75E-3	4.03E-3	1.21E-2	1.56E-2	4.92E-3	7.25E-3
$\sigma(f; 6, 96)$	7.28E-3	3.96E-3	2.93E-3	2.73E-3	1.22E-2	1.16E-2	3.63E-3	4.78E-3
$\sigma(f; 11, 91)$	7.59E-3	3.86E-3	2.44E-3	2.81E-3	1.23E-2	1.13E-2	3.39E-3	4.72E-3
$R = 0.0001$								
$\sigma(f; 1, 101)$	7.66E-3	9.02E-3	1.59E-2	7.62E-3	2.37E-2	1.91E-2	1.03E-2	1.88E-2
$\sigma(f; 6, 96)$	7.98E-3	8.65E-3	7.02E-3	6.12E-3	2.19E-2	1.57E-2	8.11E-3	1.16E-2
$\sigma(f; 11, 91)$	8.15E-3	8.28E-3	6.38E-3	5.79E-3	2.02E-2	1.53E-2	7.36E-3	1.20E-2
$R = 0.01$								
$\sigma(f; 1, 101)$	1.91E-2	7.24E-2	6.62E-2	5.60E-2	6.54E-2	7.92E-2	6.29E-2	7.50E-2
$\sigma(f; 6, 96)$	1.99E-2	7.32E-2	6.56E-2	5.42E-2	5.50E-2	7.88E-2	5.56E-2	5.14E-2
$\sigma(f; 11, 91)$	2.10E-2	7.02E-2	6.25E-2	5.51E-2	4.71E-2	7.60E-2	5.07E-2	5.64E-2

we have adopted Anderssen's labeling of the sampling grid, where $n = 1$ corresponds to the center of the object and $n = 101$ corresponds to the edge.

For clean data, Anderssen's methods give better results than the deterministic filter. This is probably because of the simple forward-difference approximation to the derivative that we used in the deterministic filter; more-accurate differentiating filters[68] may give better results. When the noise level is low, the smoothed Kalman estimates are not as good as the other methods, but, as the noise increases, they do better, and are as good or better when the noise level is high. Because of the other methods are based on numerical integration or linear algebraic equations, they should be $O(N^2)$ to $O(N^3)$, which is the same as or slower than the smoothed Kalman filter (without precomputing) for noisy data and much slower than the deterministic filter for noiseless data.

5. CONCLUSIONS

In this paper we have presented a family of new methods for Abel inversion, based on a recursive (state-variable) model of the integral transform and Kalman filter techniques for optimum least-squares estimation of the inversion from noisy data. The deterministic (exact-inverse) filter is quite fast and gives good results for noiseless data but shares with other exact-inverse methods an extreme sensitivity to noise. The Kalman filter estimates are good but tend to be biased because of the simple first-order model assumed for the object. Performing a second pass over the data with a fixed-interval smoother greatly reduces the bias and also improves the variance of the estimates, at a modest increase in computation. The Kalman filter inversion with smoothing compares favorably with the methods of Minerbo and Levy and of Anderssen, particularly when the noise levels are moderately high, and it is straightforward to implement. A further advantage of the method is that it may (in principle) be extended to process data occurring on a nonuniform sampling grid.

For readers interested in trying out these algorithms, a program coded in FORTRAN-77 is available by writing to E. W. Hansen.

ACKNOWLEDGMENTS

This research was supported by the National Science Foundation under grants ECS-8006904 and ECS-8210412. The contributions of A. Jablokow, L. Bohs, D. Farrington, W. Murray, J. Panek, and R. Wills to the early work on these methods are gratefully acknowledged.

* Current address, Digital Equipment Corporation, 146 Main Street, Maynard, Massachusetts 01754.

REFERENCES

1. R. N. Bracewell, *The Fourier Transform and Its Applications*, 2nd ed. (McGraw-Hill, New York, 1977), pp. 244–250.
2. J. C. Dainty and R. Shaw, *Image Science* (Academic, New York, 1974), pp. 210–215.
3. H. R. Griem, *Plasma Spectroscopy* (McGraw-Hill, New York, 1964), pp. 176–178.
4. W. Lochte-Holtgreven, *Plasma Diagnostics* (North-Holland, Amsterdam, 1968), pp. 184–213.
5. T. Ihjima, O. Karatsu, and I. Ogura, "Radial profiles of upper-laser-level emission in an oscillating Ar II laser," J. Appl. Phys. **47**, 383–384 (1976); "Radial profiles of upper- and lower-laser level emission in an oscillating He–Ne laser," J. Appl. Phys. **48**, 437–439 (1977).
6. R. South and B. M. Hayward, "Temperature measurement in conical flames by laser interferometry," Combustion Sci. Technol. **12**, 183–195 (1976).
7. M. Sato, "On the ion temperature determination of an inhomogeneous plasma from Doppler profiles," J. Phys. D **11**, 1739–1741 (1978).
8. R. N. Bracewell, "Strip integration in radio astronomy," Aust. J. Phys. **9**, 198–217 (1956).
9. I. J. D. Craig, "The inversion of Abel's integral equation in astrophysical problems," Astron. Astrophys. **79**, 121–127 (1979).
10. C. M. Vest, *Holographic Interferometry* (Wiley, New York, 1979), Chaps. 5 and 6.
11. C. M. Vest, "Interferometry of strongly refracting axisymmetric phase objects," Appl. Opt. **14**, 1601–1606 (1975).
12. A. Kuthy, "An interferometer and Abel inversion procedure for the measurement of the electron density profile in a cold gas-blanket experiment," Nucl. Instrum. Methods **180**, 7–16 (1981).
13. D. Marcuse, *Principles of Optical Fiber Measurements* (Academic, New York, 1981), Chap. 4.
14. S. Ugniewski, "Analysis of schlierengrams in refractometry of axisymmetric objects," Appl. Opt. **19**, 3421–3422 (1980).
15. D. C. Hammond, Jr., "Deconvolution technique for line-of-sight optical scattering measurements in axisymmetric sprays," Appl. Opt. **20**, 493–499 (1981).
16. A. J. Jakeman and R. S. Anderssen, "Abel type integral equations in stereology. I. General discussion," J. Microsc. (Oxford) **105**(2), 121–133 (1975).
17. R. S. Anderssen and A. J. Jakeman, "Abel type integral equations in stereology. II. Computational methods of solution and the random spheres approximation," J. Microsc. (Oxford) **105**(2), 135–153 (1975).
18. R. C. Jones, "On the theory of the directional patterns of continuous source distributions on a plane surface," J. Acoust. Soc. Am. **16**, 146–171 (1945).
19. A. V. Oppenheim, G. V. Frisk, and D. R. Martinez, "Computation of the Hankel transform using projections," J. Acoust. Soc. Am. **68**, 523–529 (1980).
20. E. W. Hansen and A. Jablokow, "Fast Hankel transform algorithm," J. Opt. Soc. Am. **72**, 1722 (A) (1982); E. W. Hansen, "Fast Hankel transform algorithm," IEEE Trans. Acoust. Speech Signal Process. (to be published).
21. E. W. Hansen, "New algorithms for Abel inversions and Hankel transforms," in *Proceedings of the 1983 International Conference on Acoustics, Speech, and Signal Processing* (Institute of Electrical and Electronics Engineers, New York, 1983), pp. 1260–1263.
22. See E. W. Hansen, "Theory of circular harmonic image reconstruction," J. Opt. Soc. Am. **71**, 304–308 (1982), and references therein.
23. S. J. Young, "Iterative Abel inversion of optically thick, cylindrically symmetric radiation sources," J. Quant. Spectrosc. Radiat. Transfer **23**, 479–481 (1981).
24. A. V. Clough and H. H. Barrett, "The attenuated Radon and Abel transforms," J. Opt. Soc. Am. **73**, 1590–1595 (1983).
25. G. N. Minerbo and M. E. Levy, "Inversion of Abel's integral equation by means of orthogonal polynomials," SIAM J. Numer. Anal. **6**, 598–616 (1969).
26. R. S. Anderssen, "Stable procedures for the inversion of Abel's equation," J. Inst. Math. Its Appl. **17**, 329–342 (1976).
27. T. L. Bock, "Numerical inversion of the Abel integral function, using least-squares splines," Ann. Phys. (Leipzig) **7**, 335–340 (1977).
28. W. L. Barr, "Method for computing the radial distribution of emitters in a cylindrical source," J. Opt. Soc. Am. **52**, 885–888 (1962).
29. See the historical introductions in O. H. Nestor and H. N. Olsen, "Numerical methods for reducing line and surface probe data," SIAM Rev. **2**, 200–207 (1960); H. Edels, K. Hearne, and A. Young, "Numerical solutions of the Abel integral equation," J. Math. Phys. **41**, 62–75 (1962); see also W. R. Wing and R. V. Neidigh, "A rapid Abel inversion," Am. J. Phys. **39**, 760–764 (1971).
30. O. H. Nestor, and H. N. Olsen, "Numerical methods for reducing

line and surface probe data," SIAM Rev. **2**, 200–207 (1960); H. Edels, K. Hearne, and A. Young, "Numerical solutions of the Abel integral equation," J. Math. Phys. **41**, 62–75 (1962).
31. K. Bockasten, "Transformation of observed radiances into radial distribution of the emission of a plasma," J. Opt. Soc. Am. **51**, 943–947 (1961).
32. C. J. Cremers and R. C. Birkebak, "Application of the Abel integral equation to spectrographic data," Appl. Opt. **5**, 1057–1064 (1966).
33. J. B. Shumaker, Jr., and C. R. Yokley, "The use of an analog computer in side-on arc spectroscopy," Appl. Opt. **3**, 83–87 (1964).
34. N. G. Basov, A. S. Shikanov, G. V. Sklizkov, Yu. A. Zakharenkov, D. W. Sweeney, and D. T. Attwood, "Numerical processing of interferograms of highly inhomogeneous phase objects," Sov. J. Plasma Phys. **6**, 642–645 (1980).
35. S. Ugniewski and M. Sadowski, "On numerical processing the interferograms of axially symmetric plasma discharges," Acta Phys. Pol. A **51**, 293–300 (1977).
36. H. Brunner, "The numerical solution of a class of Abel integral equations by piecewise polynomials," J. Comput. Phys. **12**, 412–416 (1973); "Global solution of the generalized Abel integral equation by implicit interpolation," Math. Comput. **28**, 61–67 (1974).
37. J. Glasser, J. Chappelle, and J. C. Boettner, "Abel inversion applied to plasma spectroscopy: a new interactive method," Appl. Opt. **17**, 3750–3754 (1978).
38. K. E. Atkinson, "The numerical solution of an Abel integral equation by a product trapezoidal method," SIAM J. Numer. Anal. **11**, 97–101 (1974).
39. E. I. Kosarev, "Applications of integral equations of the first kind in experimental physics," Comp. Phys. Commun. **20**, 69–75 (1980).
40. R. Balasubramanian, D. H. Norrie, and G. DeVries, "The application of the least squares finite element method to Abel's integral equation," Int. J. Num. Meth. Eng. **14**, 201–209 (1979).
41. G. M. Robbins and T. S. Huang, "Inverse filtering for linear shift-varying imaging systems," Proc. IEEE **60**, 862–872 (1972).
42. A. A. Sawchuk, "Space-variant image motion restoration by coordinate transformations," J. Opt. Soc. Am. **65**, 138–144 (1974).
43. D. Psaltis and D. Casasent, "Deformation-invariant optical processors using coordinate transformations," Appl. Opt. **16**, 2288–2292 (1977).
44. E. W. Hansen and J. W. Goodman, "Optical reconstruction from projections via circular harmonic expansion," Opt. Commun. **24**, 268–272 (1978).
45. D. R. Mook, "An algorithm for the numerical evaluation of the Hankel and Abel transforms," IEEE Trans. Acoust. Speech Signal Process. **ASSP-31**, 979–985 (1983).
46. P. P. B. Eggermont, "Tomographic reconstruction on a logarithmic polar grid," IEEE Trans. Med. Imaging **MI-2**, 40–48 (1983).
47. D. Casasent and D. Psaltis, "Accuracy and space-bandwidth in space-variant optical correlators," Opt. Commun. **23**, 209–212 (1977).
48. E. W. Hansen, "Circular harmonic image reconstruction: experiments," Appl. Opt. **20**, 2266–2274 (1981).
49. T. Kailath, *Linear Systems* (Prentice-Hall, Englewood Cliffs, N.J., 1980).
50. T. Kailath, *Linear Systems* (Prentice-Hall, Englewood Cliffs, N.J., 1980), Chap. 9.
51. E. W. Hansen and A. Jablokow, "State variable representation of a class of linear shift-variant systems," IEEE Trans. Acoust. Speech Signal Process. **ASSP-30**, 874–880 (1982).
52. A. Jablokow, *New Algorithms for a Class of Integral Transforms*, M.S. thesis (Dartmouth College, Hanover, N.H., 1982) (unpublished).
53. M-Y. Wu, "Transformation of a linear time-varying system into a linear time-invariant system," Int. J. Control **27**, 589–602 (1978).
54. T. Kailath, *Linear Systems* (Prentice-Hall, Englewood Cliffs, N.J., 1980), p. 601.
55. M-Y. Wu and A. Sherif, "On the commutative class of linear time-varying systems," Int. J. Control **23**, 433–444 (1976).
56. In previous descriptions of this method,[21,51,57] we let $R_0 = n\Delta$ and $R = (n-1)\Delta$ in Eqs. (15)–(18), which resulted in a backward recursion $x_{n-1} = \Phi_n x_n + \Gamma_n f_n$ for the state vector in Eq. (15), etc. The notation has been changed to bring the equations into line with common practice and make the subsequent Kalman filter exposition clearer.
57. E. W. Hansen and P-L. Law, "Abel inversion by Kalman filtering," in *Proceedings of the 1984 International Conference on Acoustics, Speech, and Signal Processing* (Institute of Electrical and Electronics Engineers, New York, 1984), Vol. 2, pp. 28B.5.1–28B.5.4.
58. B. D. O. Anderson and J. B. Moore, *Optimal Filtering* (Prentice-Hall, Englewood Cliffs, N.J., 1979).
59. J. M. Mendel, *Optimal Seismic Deconvolution—An Estimation-Based Approach* (Academic, New York, 1983).
60. N. E. Nahi, "Role of recursive estimation in statistical image enhancement," Proc. IEEE **60**, 872–877 (1972).
61. A. Habibi, "Two-dimensional Bayesian estimate of images," Proc. IEEE **60**, 878–883 (1972).
62. J. W. Woods and V. K. Engle, "Kalman filtering in two dimensions: further results," IEEE Trans. Acoust. Speech Signal Process. **ASSP-29**, 188–197 (1981).
63. The use of R to denote measurement noise covariance should not be confused with the earlier use of R as a radius.
64. B. D. O. Anderson and J. B. Moore, *Optimal Filtering* (Prentice-Hall, Englewood Cliffs, N.J., 1979), p. 111.
65. J. M. Mendel, *Optical Seismic Deconvolution—An Estimation-Based Approach* (Academic, New York, 1983), p. 71.
66. B. D. O. Anderson and J. B. Moore, *Optimal Filtering* (Prentice-Hall, Englewood Cliffs, N.J., 1979), Chap. 7; J. M. Mendel, *Optimal Seismic Deconvolution—An Estimation-Based Approach* (Academic, New York, 1983), pp. 61–66.
67. G. J. Bierman, "Fixed-interval smoothing with discrete measurements," Int. J. Control **1**, 65–75 (1973); see also J. M. Mendel, *Optimal Seismic Deconvolution—An Estimation-Based Approach* (Academic, New York, 1983), pp. 62–66.
68. L. R. Rabiner and R. W. Schafer, "On the behavior of minimax relative error FIR digital differentiators," Bell Syst. Tech. J. **53**, 333–361 (1974).